SMU Journal of Undergraduate Research

Volume 7 | Issue 1 Article 3

January 2022

The Use of Ruthenium Complexes as Molecular Probes for Non-Canonical DNA

Eleni Sullivan
Southern Methodist University, ersullivan@smu.edu

The Use of Ruthenium Complexes as Molecular Probes for Non-Canonical DNA

Eleni Sullivan

ersullivan@smu.edu

Dr. Fredrick Olness[1]

ABSTRACT

This study considered the preparation of a new DNA binding Ruthenium polypyridyl complex possessing an infrared active nitrile group. The binding abilities of a novel Ruthenium complex, [$Ru(TMP)_2DPPZ$-10-CN], to various forms of DNA—both canonical and non-canonical—were examined by performing multiple DNA titrations. DNA is of great interest as it is the carrier of genetic information for all living things. Damage to DNA can have drastically detrimental effects, so the study of its structure and replication is of great importance. Two non-canonical structures that are important are the G-quadruplex and i-motif which form at the telomeric and regulatory regions of genes, respectively, and have the ability to block telomerase activity and influence transcription. The complex was synthesized by microwave irradiation and purified using a silica column and an ion exchange with Amberlite 402. Six titrations were, then, performed with salmon sperm dsDNA, guanine monophosphate (GMP), $G_4T_4G_4$, human telomere G-quadruplex, i-motif C_5T_3, and i-motif C_{30}. The complex was found to favor non-canonical structures, particularly the G-quadruplex structure, because of its high [bp]/[Ru] concentrations. The higher concentration of base pairs or structures per Ruthenium molecule indicated that the complex had a high binding affinity for that particular DNA structure. These results support the notion that Ruthenium metal complexes can be used for theragnostic purposes and can be used to target the telomeric region of genes where G-quadruplex structures can be found and influence transcription initiation and inhibit telomerase activity.

1. INTRODUCTION

1.1 DNA

The discovery of DNA as the genetic blueprint for all organisms has contributed to many different aspects of life including medical advancements like DNA-based therapies, use in judicial law, and agricultural applications. Frederich Miescher was the first person to observe DNA in the 1800s, but its function was not proposed until 1944 when Oswald Avery showed that DNA carried the genetic information. This theory was not widely believed because its structure seemed too simple to be able to code for such complex organisms. It was not until 1953 when Watson, Crick, Wilkins, and Franklin determined DNA's double-helical structure that this theory became widespread *(17)*. This structure allows DNA to copy itself during cell division, be used as a template for transcription, and, ultimately, produce proteins.

1.2 DNA Structure

The structure of DNA consists of an antiparallel, carbon-phosphate backbone with complementary base pairing of nucleotides. Its chemical polarity distinguishes between the two ends of the chain—5' phosphate and 3' hydroxyl—and is an important factor in DNA replication and transcription *(18)*. The complementary base pairing allows for the most energetically favorable conformation, shaping the backbone into an antiparallel double helix with major and minor grooves where molecules can bind and influence different biological processes *(1)*, see **Figure 1** below.

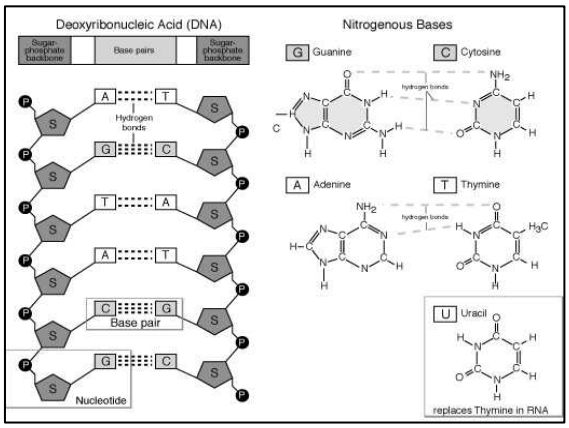

Figure 1: DNA Structure *(24)*.

1.3 Different Forms of DNA

While the double stranded, B-DNA shape is the most common form of DNA, it can adopt other forms depending on its environment. A-DNA and B-DNA are both right-handed helical structures, but A-form is thicker and has a shorter distance between the base pairs. Since B-form has a wider major groove, it can make specific contact with amino acids in DNA-binding proteins. Contrastingly, Z-

[1] Professor of Physics at Dedman College

DNA is left-handed and formed by alternating long sequences of pyrimidines and purines. It is believed that this form of DNA plays a role in the regulation of cellular functions *(10)*. G-quadruplexes are four stranded structures with a single Guanine-rich strand and a complementary Cytosine-rich hairpin, an i-motif structure, that make up the major structural region at eukaryotic telomeres or lie close to the promoter regions—both could be necessary for gene regulation and transcription initiation *(22)*, as shown in Figure 1 of "Metal-Based Drug-DNA Interactions" *(8)*[2].

1.3.1 I-Motif DNA

I-motifs are four stranded DNA complexes formed by cytosine rich strands found in regulatory regions of the genome, supporting the claim that i-motifs play a role in gene expression. Their hemi-protonated C:C$^+$ pairing is the key element in the i-motifs stability (refer to **Figure 3 a**) and it is known that their formation is higher during transcription than in DNA replication. These i-motif structures, depending on sequence, can be formed at mildly acidic and neutral pH—typically around a pH of 5.5-5.7. IMC-76 and IMC-48 are two small molecules that bind to and stabilize hairpin and i-motif DNA structures giving them the ability to repress or activate gene expression, see Figure 2 b and c below. A study with the Bcl2 oncogene showed that IMC-48 promotes stability of the i-motif structure and upregulation of Bcl2, whereas IMC-76 stabilizes the hairpin species of the Bcl2 gene resulting in transcriptional repression in lymphoma cell lines. This study reinforces the idea that i-motif structures play a role in gene expression, particularly with transcription initiation *(3)*.

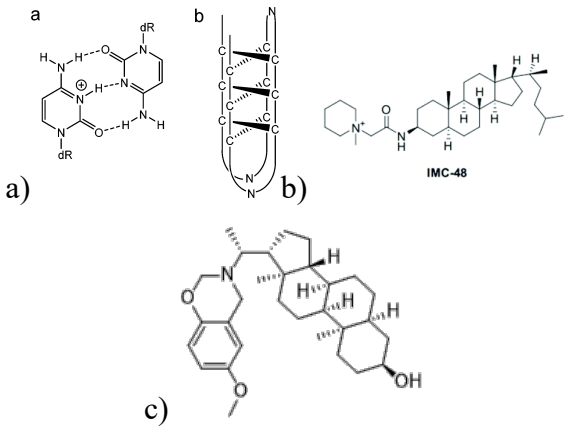

Figure 2: a) I-Motif Structure b) Structure of IMC-48 c) Structure of IMC-76 *(3)*

1.3.2 G-Quadruplex DNA

G-quadruplex DNA has also been found to play a role in the regulation of gene expression because of its ability to block telomerase activity and inhibit or promote transcription *(5)*. These structures consist of two or four separate DNA strands that can exist in different conformational combinations. These variations result from loop size, strand direction, and sequence, as shown in **Figure 3**. The structure forms tetrads of DNA stacked on top of one another that are held together by loops of varying sequences. As seen in **Figure 4**, the loops cause the formation of different parellelities—antiparallel, parallel, and a hybrid of the two. The formation of these structures is, also, dependent on cations: Na^+ can exist in one plane or between two adjacent tetrads, whereas the K^+ ions are equidistant between the tetrads *(22)*. For example, it has been shown that telomerase, an overexpressed enzyme in ~85% of cancer cells, is inhibited if single-stranded telomeric DNA is folded into a G-quadruplex structure. Telomerase is an enzyme that proliferates DNA by extending the telomere that exists at the ends of chromosomes. If telomerase is overactive, as it is in most cancerous cells, then the cell will become immortal. Also, it has been found that the promoter regions of certain oncogenes are G-rich, and the formation of G-quadruplexes in these regions is thought to have an impact on the oncogene's transcription *(23)*. Under normal conditions, the G-rich content found in the promoters of oncogenes regulates the oncogenes so that they do not create cancerous cells, but overexpression and mutations can cause those oncogenes to create cancerous cells. G-quadruplex structures lead to telomere uncapping and release of telomere-binding proteins which signals a DNA damage response, ultimately ending in apoptosis. A new method is being tested to see if antiparallel G-quadruplex structures, which block telomerase, could act as an anti-cancer therapy treatment. Experimentation is being done with these G-quadruplex structures and different ligands to find a complex that promotes the formation of these antiparallel G-quadruplexes in the hopes that they might inhibit telomerase and consequently kill malignant cancer cells *(5)*.

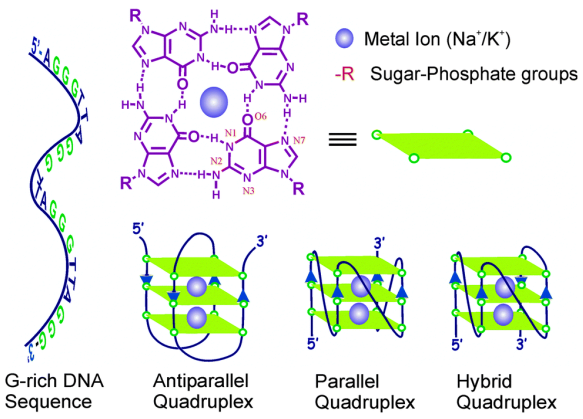

Figure 3: G-Quadruplex Structure *(4)*

1.4 Binding Interactions with DNA

With these different DNA structures come different molecular interactions with the DNA in terms of their binding modes. There can be direct and indirect binding by proteins which determines the binding selectivity of the molecule. Through direct binding, individual bases make

[2] The figure referenced above would have been reprinted, however permission could not be attained.

direct contact with the protein's surface. In this type of binding, the DNA-binding motif is inserted into the major groove of the DNA molecule. The exposed side chains in the major groove are different from that of the minor group distinguishing the two groove binding spots—the major groove exposes more sequence information because of charge pattern differences making it easier to bind to than the minor groove. DNA intercalation, shown in Figure 4 below, is the process of inserting molecules between the base pairs of DNA, like many metal complexes. The DNA must unwind in order to accommodate ligands into the backbone, and these intercalators are typically synthesized for use in chemotherapeutic treatment, such as ruthenium, rhodium, and iridium, because they can inhibit DNA replication in rapidly growing cancer cells. Electrostatic interactions appear between base pairs of the DNA alpha helix as well as play a role in ligand intercalation into the DNA duplex. Major and minor groove binding is distinct because of the position of the backbone in the major and minor grooves of DNA. The backbone is farther apart in the major groove than in the minor groove, and the distance between the backbones in the major grooves makes it easier for ligands to bind as opposed to the minor groove, although ruthenium complexes have been found to intercalate into the minor groove.

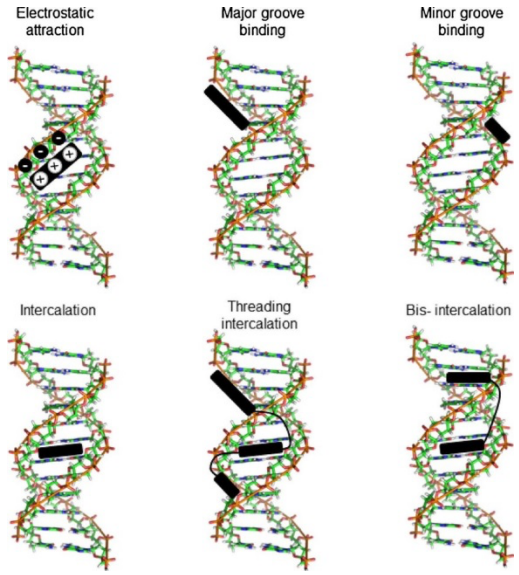

Figure 4: Binding Modes to B-DNA

1.4.1 I-Motif DNA

The binding ligands associated with the i-motif structure stabilize the motif but are not selective, as they will bind with other DNA structures. I-motif binding ligands are not as definitive as those of G-quadruplexes, but those such as TMPyP4, BisA, and phenanthroline derivatives have been described as ligands for the i-motif structures. Ruthenium and terbium metals are, also, potential i-motif binders, but they lack specificity and slightly destabilize the structure. Carboxyl-modified single-walled carbon nanotubes (C-SWNTs) are the first selective i-motif ligands binding the 5'end of the major groove of the telomeric structure. These structures of C-SWNTs bound to i-motif structures can inhibit telomerase activity, interfere with telomere functions, and lead to apoptosis in cancer cells as well as inducing the formation of G-quadruplex structures on the complementary G-rich strand. As previously mentioned, IMC-48 binds and stabilizes the i-motif structure found in the BCL2 gene promoter activating gene expression whereas IMC-76 suppresses levels of BCL2. The BCL2 activating transcription factor, hnRNP LL, also shows an affinity for the i-motif structure formed by the BCL2 promoter oncogene, this sequence is shown below in **Figure 5** *(3)*. Different pHs can also affect the stability of i-motif structures and can be used as manipulators in order to form the structures experimentally.

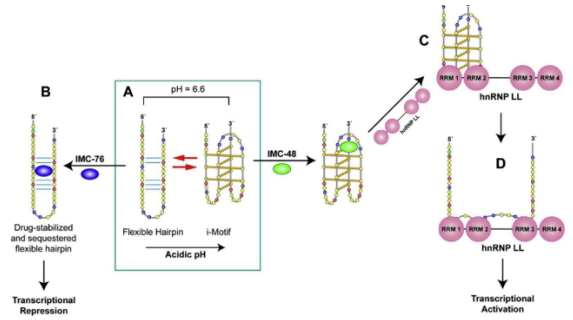

Figure 5: Proposed Model of IMC-76 and IMC-78 Binding with I-Motif DNA *(26)*

1.4.2. G-Quadruplex

G-quadruplex binding ligands are small molecules that may affect the formation and unfolding of G-quadruplex structures during transcription to either enhance or representative the progression of transcription, as shown in **Figure 7** below. These ligands typically bind at the G-quartets found at the end of G-quadruplexes; however, small molecules have the ability to also bind to nucleotides on the loops that do not participate in the G-quadruplex structures, but rather link the tetrad structure together and determine their formation. Four binding modes are shown below in **Figure 6**: the typical (or native) ligand-quadruplex complex, four ligands bound simultaneously to the G-quartets and loops, two ligands bound to separate ends of the G-quadruplex, and two ligands bound separately to different ends of the structure's loops. A concern for these ligands is that they may affect the flexibility of the G-quadruplex structure as well as block the binding interaction between G-quadruplexes and their binding proteins because they also tend to bind to the loops outside of the tetrad structure. This, however, opens up an opportunity for the creation of drugs that target the loops of G-quadruplex structures. These drugs could bind where the G-quadruplex proteins would usually bind and give them the ability to block the protein's function and, ultimately, blocking telomerase activity of cancerous cells *(25)*.

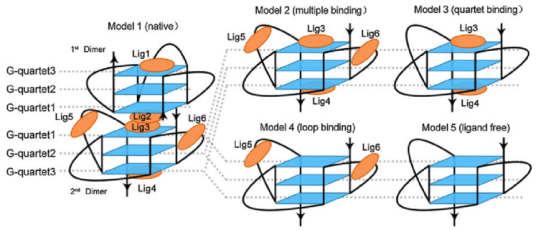

Figure 6: Proposed Binding Methods of Ligands to G-Quadruplex Structure *(25)*

1.5 Binding Interactions between Molecules and DNA

Interactions between molecules and DNA can occur through covalent and non-covalent binding techniques. Covalent binding is irreversible, completely blocking DNA function and causing cell death. Non-covalent binding—intercalation, electrostatic interactions, and groove binding—is reversible and typically targets the minor groove of DNA. Metal complexes, like cisplatin are known to covalently bind DNA via interstrand crosslinking. This crosslinking has a high binding strength, and these adducts disturb protein recruitment that is crucial for transcription and replication, which is why they are an interesting subject of potential anticancer treatments *(2)*. Organic intercalators, like Ruthenium complexes, can also be used in anticancer treatments because the polyaromatic compounds slide in between two adjacent base pairs and inhibit DNA replication in a reversible fashion *(21)*.

1.5.1. Metal Complexes

Metal complexes are known to interact strongly and selectively with the loops and grooves in G-quadruplex structures *(9)*. Each transition metal complex's structure and chemical properties allow for specific interactions with DNA and for a more selective approach to targeting molecules. The center ions in metal complexes also form different G-quadruplex structures, changing and affecting their binding abilities and specificities. Cisplatin, for example, covalently binds to DNA, forming adducts because of the chloride sites within the complex that are aquated whereas ruthenium complexes do not covalently bind, they bind reversibly by intercalating into the minor groove of the DNA molecule. Metal complexes were found to bind DNA to stop replication and induce apoptosis with square planar complexes allowing for deeper insertion into the DNA as compared to octahedral or tetrahedral structures *(19)*. It is because of these properties that metal complexes are being proposed as G-quadruplex DNA binders due to their highly efficient binding specificity on the pi-pi stacking planar core *(23)*. They also often possess distinctive electrochemical or photophysical properties that enhance the functionality of the binding agent. It was found that complexes bound to ligands such as dpphen, tpy, or dppz were able to bind more efficiently depending on its target's chemical properties and binding location, as seen in **Figure 7** below *(16)*. Because of metal complexes' photophysical properties, their specificity and high binding affinity, they are efficient probes for G-quadruplex DNA *(9)*.

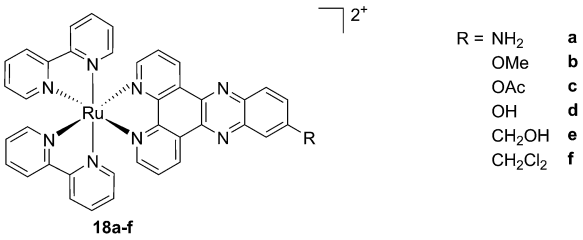

Figure 7: Ruthenium complex bound to a dppz ligand *(15)*

1.5.2. Ruthenium Complexes

Ruthenium complexes, in particular, have the ability to bind more selectively to cancerous cells as opposed to current chemotherapy drugs. These are of interest because of their versatility—they can be bound to a wide variety of ligands, some of which can intercalate more deeply than others making them more effective binders (refer to **Figure 8** below). It also has a high cytotoxicity with cancer cells and low cytotoxicity with healthy tissue—unlike cisplatin *(7)*, and a strong metal-to-ligand-charge-transfer in hydrophobic environments, like the inner space of the DNA alpha helix, but not in aqueous environments because of the hydrogen bonds that form between nitrogen and the surrounding water molecules. The Ruthenium-dppz complex has distinct photophysical properties that are evident when intercalated into the grooves of DNA. This "light switch effect" allows the complex to act as a probe for DNA because a strong luminescence is emitted from a solution containing ruthenium complexes and G-quadruplex DNA. An emitted light indicates that the ring nitrogens of the dppz ligand are shielded from the aqueous environment through intercalation into the DNA base pair stack *(16)*.

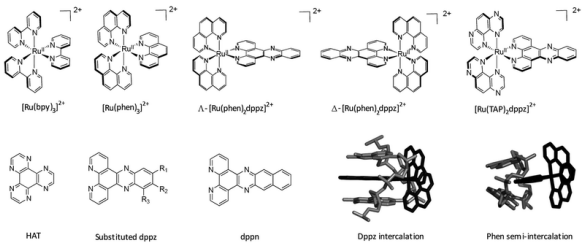

Figure 8: Various structures of ruthenium complexes with various extended ligands and their intercalation *(27)*

1.6 Structure of Ruthenium Complexes

The structures of ruthenium complexes are stable, versatile, and well known, which is why they have been tested for anticancer therapy. The complexes that have gone into trial have exhibited an ability to prevent metastasis formation and inhibit preexisting advanced tumors with relatively low toxicity. The structure has two enantiomers: delta and lambda, as shown in **Figure 9** below. The delta enantiomer has been found to bind via intercalation, whereas the lambda enantiomer seems to prefer binding to the DNA groove. They can both, however, covalently bind to DNA and intercalate into the minor groove, and their chiral properties can influence biological activity depending on the isomer *(19)*.

1.7 Chirality

Chirality is an important aspect of biological systems so the mechanisms and anticancer activities of the ruthenium polypyridyl complex enantiomers—delta and lambda—is of great interest *(7)*. Since DNA has a chiral double-helical structure, enantiomers can have different binding abilities and a high level of discrimination between left-handed and right-handed DNA, which makes them perfect for selective targeting of cells (refer to **Figure 10** below). There is evidence that certain chiral metal complexes have the ability to not only distinguish between the handedness of DNA before intercalating into the DNA, but also change the shape of the DNA to the chiral form preferred by each ligand *(20)*.

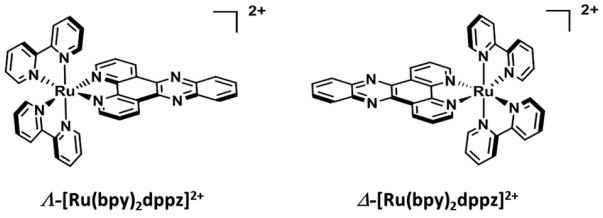

Figure 9: Ruthenium Complex Enantiomers *(12)*

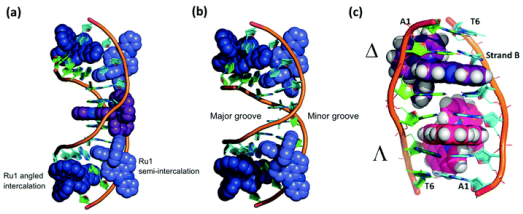

Figure 10: Ruthenium Complex Minor Groove Intercalation *(12)*

1.8 Use of Ruthenium Complexes as Probes

Ruthenium probes have been proposed for use as a photosensitizer in an emerging clinical modality—photodynamic therapy (PDT). It deals with light-matter interactions possessing an anti-tumor effect that is reliant on three components: a photosensitizer, light, and oxygen. PDT only exhibits immediate efficacy within the vicinity of the photosensitizer, which is different from the lack of selectivity that is associated with current chemotherapy treatments that can cause severe systemic toxicity. Ruthenium complexes are advantageous because of their unmatchable photostability and wide modification potential. Unfortunately, the dependence of PDT on oxygen makes it hard to penetrate into deep tissue, so the search for ruthenium complexes with less oxygen dependence is required *(14)*. $[Ru(TMP)_2dppz]^{2+}$ exhibits a somewhat brighter emission in the presence of a DNA mismatch relative to completely well-matched DNA. It binds at the mismatch site in the minor groove through metalloinsertion. The methyl groups of tetramethyl phenanthroline (TMP) are thought to disfavor binding to well-matched sites because of steric clashing between the ancillary ligands and the DNA backbone, also its smaller size allows it to intercalate more deeply. Since these methyl groups tend to favor mismatched sites, they can be used as probes to detect mutations that could be the cause of cancerous cells. It is because of these findings that this complex has been portrayed as a potential diagnostic probe for the early detection of mismatch repair-deficient cancers *(6)*.

1.9 Project Aims

- Prepare new TMP complex with a DPPZ-CN ligand that can act as a near-infrared (NIR) probe
- Perform DNA titrations to assess the binding modes and mechanisms of the new Ruthenium-DPPZ-CN complex with different forms of DNA including double stranded DNA, G-quadruplex DNA, and i-motif DNA
- Investigate use of TMP ligand and its preference for structures

2. SYNTHESIS AND CHARACTERIZATION OF $RU(TMP)_2(DPPZ\text{-}10\text{-}CN)$

2.1 Introduction

Ruthenium complexes are of great interest because of their vast modification potential as well as their "light switch" abilities and high selectivity. A new ruthenium complex was first synthesized to be able to test out its different binding affinities to various DNA structures, both canonical and non-canonical. The synthesis was performed according to established literature with the ruthenium precursor, $Ru(TMP)_2Cl_2$—refer to **Scheme 2.1** for its synthesis, being attached with a ligand, DPPZ-10-CN, in an attempt to create a novel complex, see **Scheme 2.2**.

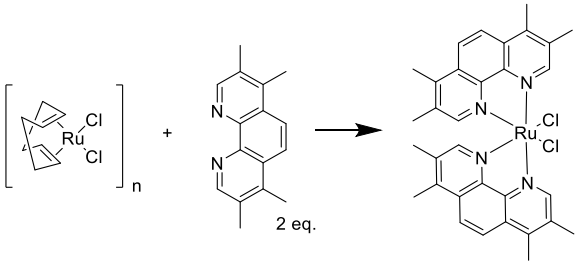

Scheme 2.1: Synthesis of Ruthenium complex precursor, $Ru(TMP)_2Cl_2$

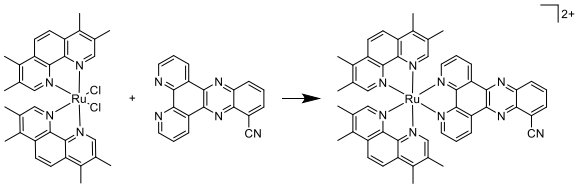

Scheme 2.2: Synthesis of novel Ruthenium complex, $[Ru(TMP)_2(DPPZ\text{-}10\text{-}CN)]^{+2}$

2.2 Results & Discussion

The synthesis of the complex was first attempted using ethylene glycol and previous literature preparation; however, this was unsuccessful. The reaction was repeated using solvent conditions of equal parts water and ethanol. The crude NMR indicated presence of impurities and so

column chromatography was performed using an SiO column. The eluent for the chromatography column was determined by testing different eluents with TLC plates. A clear separation of the components was desired from the various eluents tested in order to purify the product. An image of the column chromatography performed is pictured below in **Figure 2.1 b**. The selected product from the fractions collected was further purified by performing an ion exchange using Amberlite 402 from the $(PF_6)_2$ salt, soluble in organic solvents, to Cl_2, so that it could be soluble in water and used in the DNA titrations; however, it is also a useful technique to get rid of some of the impurities seen in the H-NMR.

After heating using microwave irradiation and purifying the product complex, ^{1}H-NMRs were performed on two sets of combined fractions collected from a silica column. The results, as shown below in **Figure 2.1 a,** show that the complex can be found in fractions 1 through 4. While the number of protons found in the aromatic region was 19, not 17, the methyl protons added up to the expected number, 24, and the other peaks can be attributed to impurities. The other fractions collected, five and six, had the predicted number of protons in the aromatic region, 17, but were missing protons in the methyl group region with only 17; refer to the **Appendix**.

a)

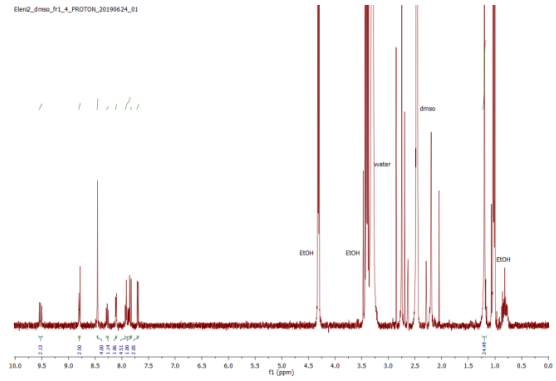

b)

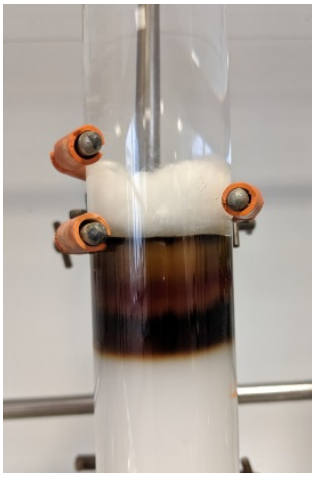

Figure 2.1 a) H-NMR Spectroscopy Data of Fractions 1-4 b) SiO Column of Complex

In **Figure 2.2**, the infrared (IR) of the complex $Ru(TMP)_2DPPZ$-10-CN shows that the nitrile band that was intended to attach to the complex is present in the structure at wavenumber 2232 cm^{-1}. The vibrations between 1300-1600 cm^{-1} are due to the polypyridyl ligands. This characterization test confirms that the desired nitrile group has attached to the structure of the complex.

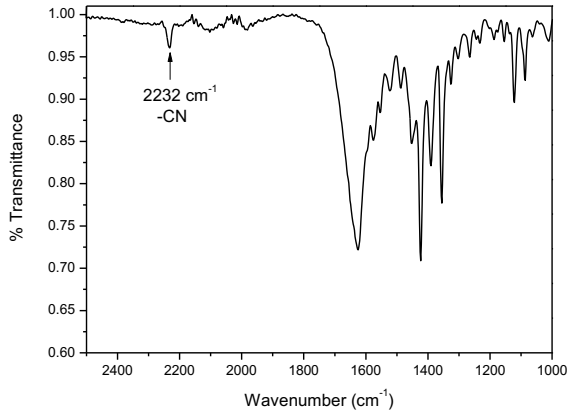

Figure 2.2 Infrared Radiation Spectrum with Indicated Nitrile Group, -CN

The complex's emission and absorbance spectrums were also recorded using the UV-Visible, as seen below in **Figure 2.3**. The MLCT band can be seen at a wavelength of 420 nm and the DPPZ band can be seen at wavelength 380 nm, as indicated by the blue line. These two bands are the regions that will change in response to additions of DNA. This particular ruthenium complex, as expected, did not emit much light, as shown by the red trend line, with the intensity staying between 0.0 and 0.04, when executed at the MLCT II.

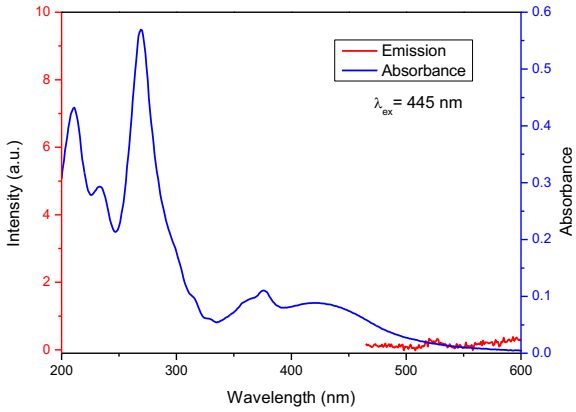

Figure 2.3 Emission and Absorbance Spectra of $Ru(TMP)_2DPPZ$-CN, excited at 445 nm

2.3 Conclusion

In conclusion, the microwave reaction seemed to have synthesized the desired $Ru(TMP)_2DPPZ$-10-CN complex as opposed to the solvothermal reaction. Both

reactions were performed the same way except for the initial reaction at slightly varying temperatures, microwaving at 140°C versus refluxing at 135°C; and using different solvents, a ratio of equal parts water and ethanol instead of ethylene glycol. This suggests that microwaving the reaction at 140°C and using equal parts water and ethanol is a more effective way to produce this particular ruthenium complex. It is expected that with the addition of the nitrile group, CN, onto the C-10 position, the complex will be able to act as an efficient IR probe. The addition of this nitrile group also, as expected, quenches the emission of the complex, preventing it from behaving according to the "light switch" effect found with other ruthenium complexes.

3. BINDING INTERACTIONS OF $Ru(TMP)_2(DPPZ\text{-}CN)$ WITH VARIOUS DNA FORMS

3.1 Introduction

The binding interactions of small molecules, focusing on $Ru(TMP)_2(DPPZ\text{-}10\text{-}CN)$ in this project, to the various non-canonical forms that B-DNA adopts is of particular interest because of their roles in gene expression, specifically transcription and replication. The G-quadruplex structure, composed of stacks of guanine tetrads, forms at the telomeric region of DNA and has the ability to block telomerase activity and inhibit transcription. The i-motif structure, made up of hemi-protonated cytosines, is found in regulatory regions of genes and plays an important role in transcription initiation. UV-Visible titrations are an effective way to monitor interactions with DNA. The DNA does not absorb in the visible region—absorbing at 260 nm, therefore, changes in the environment of the complex as it moves from solution to DNA bound are reflected in changes in the MLCT band at 420 nm and DPPZ band at 380 nm (refer to **Figure 3.1** below). Multiple titrations were performed in order to compare the created ruthenium complex's binding affinity for these various non-canonical DNA forms.

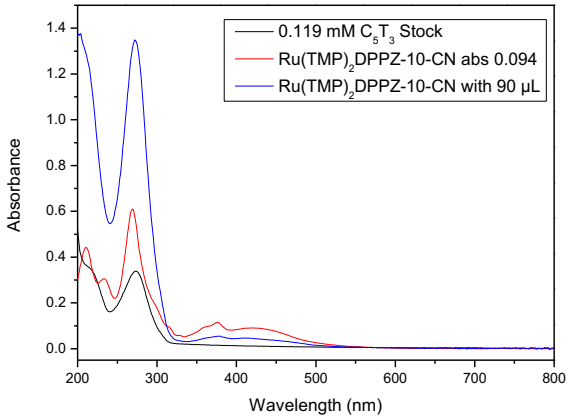

Figure 3.1 UV-Visible of DNA vs. Complex vs. DNA in solution with complex

Four different types of non-canonical DNA were used in this study: $G_4T_4G_4$, human telomere G-quadruplex, $(C_5T_3)_4$ i-motif structure, and C_{30} i-motif structure. The $G_4T_4G_4$ structure is a bimolecular, antiparallel G-quadruplex structure and the human telomere G-quadruplex (GGGTTA) is an intramolecular structure found in the telomeric regions of DNA. These two structures acted as the non-canonical examples of G-quadruplex DNA. The intramolecular $(C_5T_3)_4$ and C_{30} i-motif structures form loops and consist of four C_{30} strands coming together, respectively, and represent the i-motif structure samples used.

3.2 Comparison of Binding Interactions of $Ru(TMP)_2(DPPZ\text{-}10\text{-}CN)$ with Salmon Sperm DNA and GMP

3.2.1 Salmon Sperm DNA

To test the complex's binding affinity for typical B-form DNA, the first titration was performed using dsDNA from salmon sperm at a stock concentration of 0.782 mM. A gradual, declining slope can be seen when examining the data, shown in **Figure 3.1 (a) and (b)** below, indicating that the complex is interacting with the SS DNA. There is also a shoulder that exists in the left peak of the MLCT band that disappears as the concentration of DNA is added, suggesting that there is a change in the environment. The curve on the right peak also narrows and loses its smooth bend. The slow decrease seen in **Figure 3.1 b** implies that while the complex shows an affinity for the salmon sperm DNA, it is a weak affinity as it does not bind as rapidly as it would if there was a strong attraction.

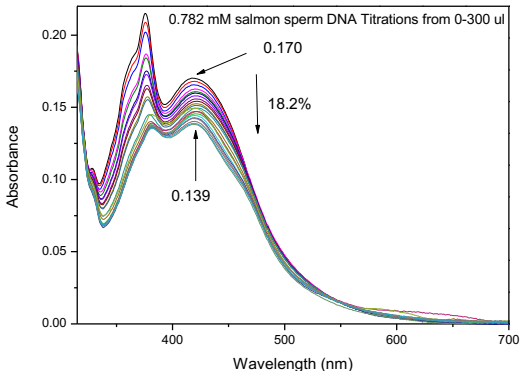

a)

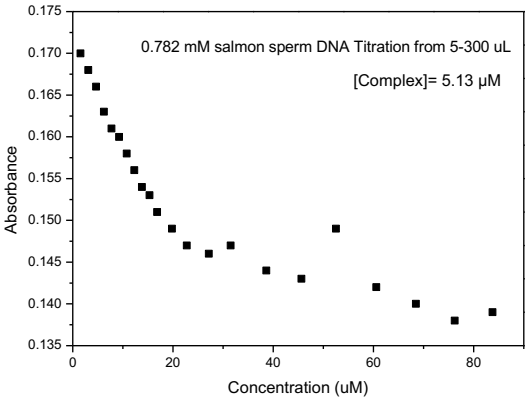

b)

Figure 3.1 a) Absorbance Graph Using UV-Visible Spectroscopy of 0.782 mM salmon sperm DNA and [Complex]= 5.13 µM b) Maximum Absorbance Points at Wavelength 420 nm

This same titration was repeated using a more concentrated stock of salmon sperm DNA at 1.98 mM, as seen in the absorbance graphs in **Figure 3.2** below. The absorbance of the ruthenium complex is lower, 0.0974, when using the more concentrated DNA stock as compared to the absorbance used when titrating with the 0.782 mM stock solution. This gives a more drastic initial decrease and causes the absorbance to plateau much sooner, at 100 uL, than with the less concentrated sample, at 300 uL. As with the previous salmon sperm titration, there is a shoulder that disappears on the left peak and the peak at 381 nm drops below the right band's peak at 420 nm. The curve on the right peak also narrows and loses its smooth bend, as seen below in **Figure 3.1 a**. These characteristics suggest that there is a change in the environment of the solution. Looking at **Figure 3.2 b**, at the peak there are 0.922 base pairs of salmon sperm DNA per complex which shows a good affinity for the salmon sperm DNA with a 50% decrease seen when there are 0.5 base pair equivalents.

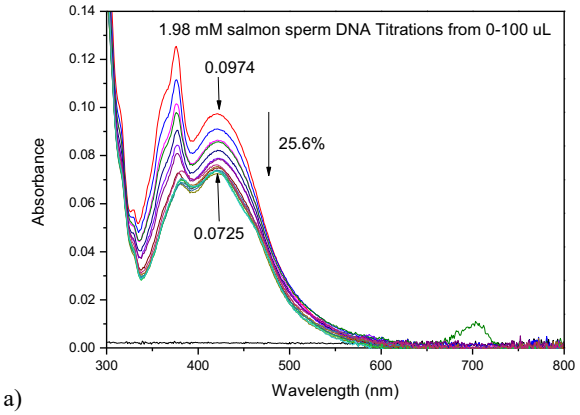

a)

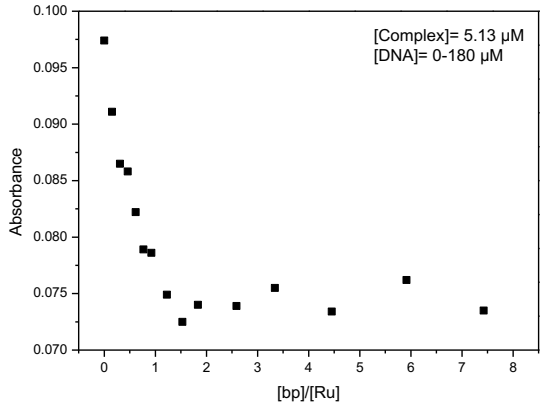

b)

Figure 3.2 a) Absorbance Graph Using UV-Visible Spectroscopy of 1.98 mM salmon sperm DNA and [Complex]= 5.13 µM b) Ratio of [bp]/[Ru]

3.2.2. Guanine Monophosphate (GMP)

The titration appears uniform as the concentration of DNA increases with the MLCT and DPPZ band's highest and lowest peaks decreasing steadily. The shoulder on the left peak that is seen at the beginning of the titration, in **Figure 3.3 a,** does not disappear as was the case with the salmon sperm titrations. Both peaks maintain a steady decrease at the same wavelength throughout the titration until completion; this could mean that there is interaction with the GMP, as seen by the significant hyperchromism. **Figure 3.3 b** shows that the solution reaches saturation at 27.5 [bp]/[Ru], again suggesting interaction in solution.

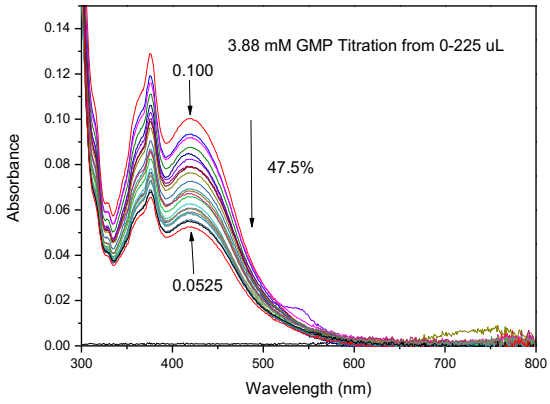

a)

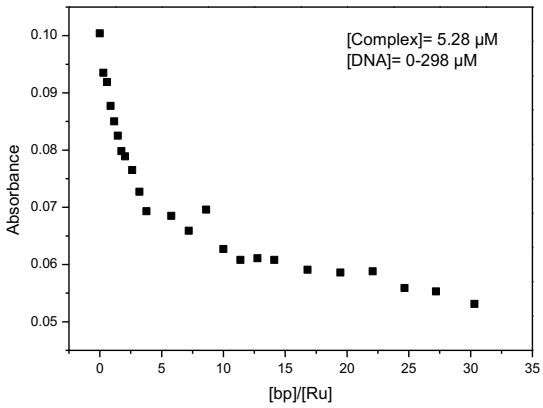

b)

Figure 3.3 a) Absorbance Graph Using UV-Visible Spectroscopy of 3.88 mM GMP and [Complex]= 5.28 µM b) Ratio of [bp]/[Ru]

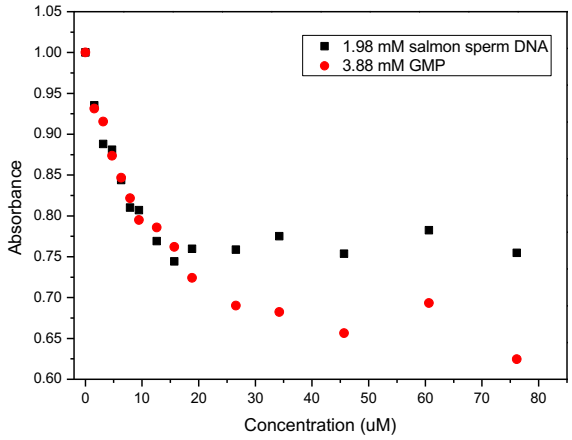

Figure 3.4 Comparison of the Concentrations of 1.98 mM salmon sperm DNA and 3.88 mM GMP, Normalized by Division of the Maximum

3.3 Comparison of Binding Interactions of Ru(TMP)$_2$(DPPZ-10-CN) with G$_4$T$_4$G$_4$, Human Telomere G-Quadruplex, C$_5$T$_3$, and C$_{30}$

These non-canonical forms of DNA consisting of different structures of G-quadruplexes and i-motifs were titrated with the synthesized Ruthenium-DPPZ-10-CN complex to test its binding affinities for the two structures. As previously mentioned, G-quadruplexes and i-motifs are important structures for gene regulation so are of interest for theragnostic purposes. In **Figure 3.9** below, the trends have been normalized and one can see that the complex favored binding to the two G-quadruplex structures as opposed to the two i-motif sequences. The hyperchromism for the titration with the human telomere G-quadruplex sequence was the highest and the titration did not reach complete saturation at the end of the titration, unlike the others, suggesting that this particular complex has a high binding affinity to this structure.

3.3.1 G$_4$T$_4$G$_4$

The complex showed a relatively high affinity for this DNA structure with a hyperchromism of 48.9%. This large hyperchromism implies that the added DNA is interacting with the complex, as shown in **Figure 3.5 a,** suggesting that the complex has an affinity for this particular G-quadruplex sequence. It should be noted that the shoulder that exists on the left peak as well as the peak of the right band broaden with the addition of DNA. The ratio of the highest peaks decreases with the addition of DNA, as well, starting at 1.25:1 and ending at 1.08:1. This change in ratio can also be an indicator of a change in environment. The high concentration of [Quadruplex]/[Ru], reaching saturation at 0.218 [Quadruplex]/[Ru], implies that the ruthenium complex favors this G-quadruplex structure sequence, as seen in **Figure 3.5 b** below.

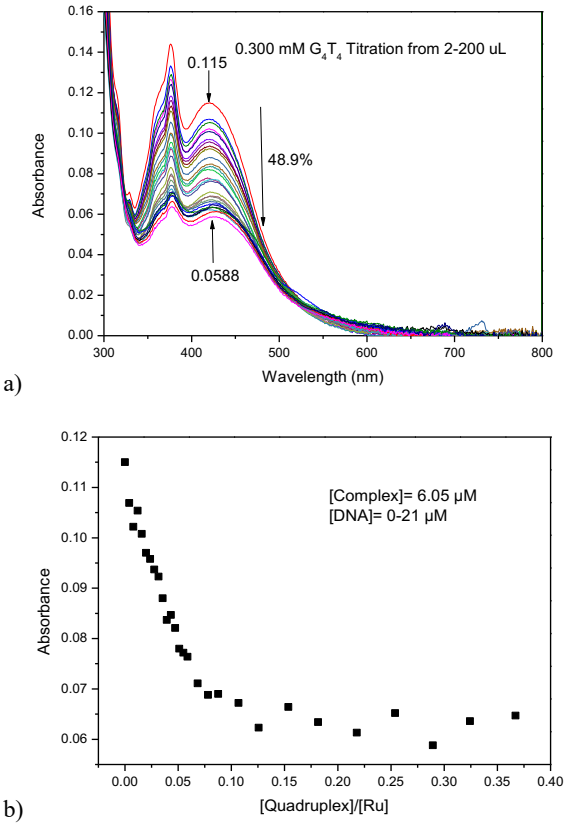

Figure 3.5 a) Absorbance Graph Using UV-Visible Spectroscopy of 0.300 mM G$_4$T$_4$ and [Complex]= 6.05 µM b) Ratio of [Quadruplex]/[Ru]

3.3.2 Human Telomere G-Quadruplex

As compared to the G$_4$T$_4$ absorbance graph, the binding affinity of the Ruthenium-DPPZ-10-CN complex to the human telomere G-quadruplex appears to be much stronger. As shown in **Figure 3.6 a and b**, it appears that the Ruthenium-DPPZ-CN complex favors the human telomere G-quadruplex DNA sequence based off the hyperchromism of 54.7%. **In Figure 3.6 a,** the shoulder of the left peak becomes more defined and the right peak widens as the concentration of DNA increases. The ratio of the highest and lowest peaks also remains constant with the addition of DNA, as seen in the **Appendix**. Similarly to the other G-quadruplex sequence tested, it appears that this ruthenium complex favors the sequence of this structure, as well, with the complex reaching its lowest point at 0.387 [Quadruplex]/[Ru], as seen in **Figure 3.7 b** below. This titration does not reach a fully saturated solution which implies that the complex would continue to bind to the DNA if more was added.

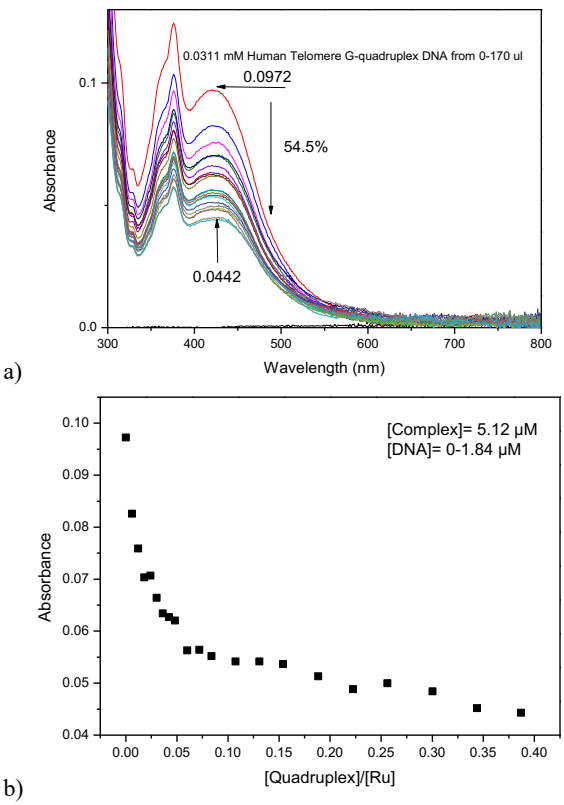

Figure 3.6 a) Absorbance Graph Using UV-Visible Spectroscopy of 0.0311 mM Human Telomere G-Quadruplex and [Complex]= 5.12 µM b) Ratio of [Quadruplex]/[Ru]

3.3.3 C_5T_3

Like the titration with human telomere G-quadruplex, there was an initial large decrease, but this graph has a smaller hyperchromism indicating that the complex favored binding to the human telomere G-quadruplex structure as opposed to the C_5T_3 i-motif structure. Similar to previous graphs, the shoulder on the left peak of the MLCT band remains constant, but the peak on the right band shifts left and narrows, straightening out the trend line instead of the rounded curve observed at the beginning of the titration, as shown in **Figure 3.7 a** below. **Figure 3.7 b**, also pictured below, shows that the complex reaches its saturation point at 0.357 [i-Motif]/[Ru], about the same as the human telomere G-quadruplex structures, but the complex still seems to show a stronger affinity to that of the human telomere.

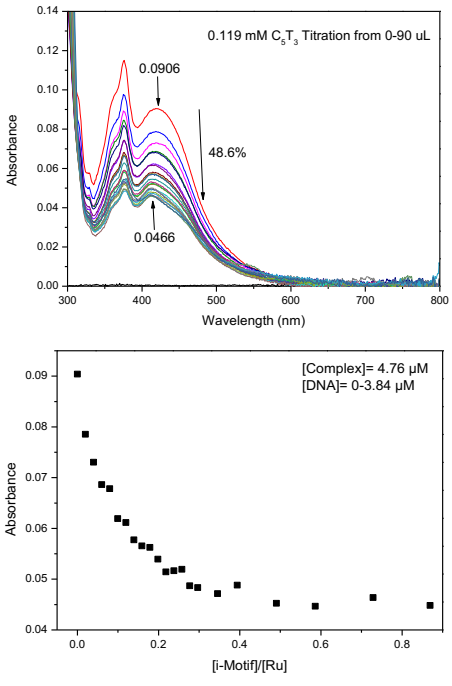

Figure 3.7 a) Absorbance Graph Using UV-Visible Spectroscopy of 0.119 mM C_5T_3 and [Complex]= 4.76 µM b) Ratio of [i-Motif]/[Ru]

3.3.4 C_{30}

This sequence had the lowest hyperchromism out of the four non-canonical sequences at 43.4%. The environment of this solution appears to remain constant because the shoulder that is observed in the left band is seen throughout the end of the titration and both peaks stay at the same wavelengths from beginning to end, as seen in **Figure 3.8 a** below. This i-motif sequence was not saturated until it reached 0.187 (refer to **Figure 3.8 b** below) which is less than all three of the other non-canonical structures tested.

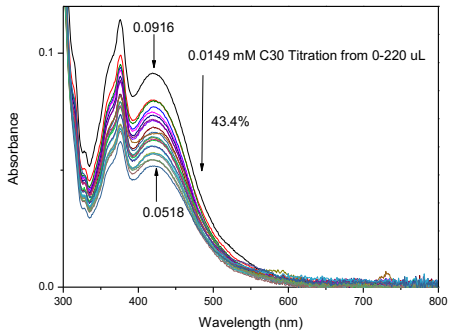

a)

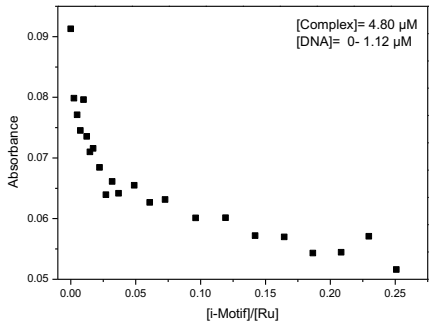

b)

Figure 3.8 a) Absorbance Graph Using UV-Visible Spectroscopy of 0.0149 mM C_{30} and [Complex]= 4.80 µM b) Ratio of [i-Motif]/[Ru]

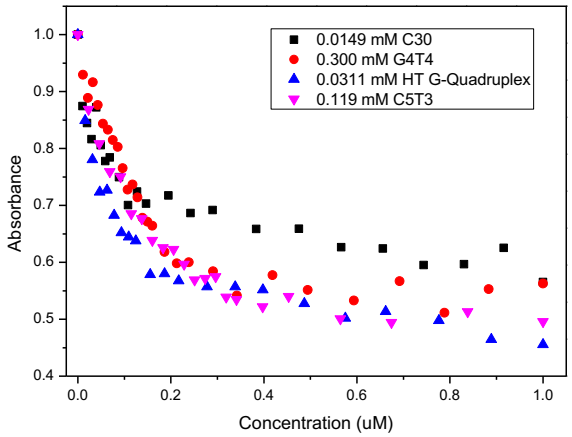

Figure 3.9 Comparisons of Titrations with G_4T_4, Human Telomere G-Quadruplex, C_5T_3, and C_{30}, Normalized by Division of the Maximum

3.4 Conclusion

In conclusion, based off of the trends exhibited by the titration data, it can be determined that the complex synthesized, $Ru(TMP)_2(DPPZ\text{-}10\text{-}CN)$, favors non-canonical forms of DNA over canonical forms of DNA. More specifically, out of the two non-canonical structures tested, it has a higher affinity for G-quadruplex structures more so than i-motif structures. However, this complex did exhibit a high affinity for the C_5T_3 i-motif structure, like that of the human telomere G-quadruplex structure. This trend suggests that while, in general, this ruthenium complex favors G-quadruplex structures, it also has a great affinity for the C_5T_3 i-motif structure. These results support the notion that ruthenium metal complexes can be used for theragnostic purposes to target the regulatory and telomeric regions of genes where i-motifs and G-quadruplexes, respectively, can be found and influence gene expression and transcription in cancerous and potentially cancerous cells.

4. MATERIALS AND METHODS

4.0 Materials

$Ru(TMP)_2Cl_2$, DPPZ-10-CN, acetone, ethylene glycol, ethanol, sodium nitrate, silica, acetonitrile, PF_6, methanol, H_2O, deoxyribonucleic acid (DNA) sodium salt from salmon testes, guanine monophosphate (GMP), G_4T_4, human telomere G-quadruplex, C_5T_3, C_{30}, 10 mM potassium phosphate buffer, 1 M potassium chloride, and potassium monobasic buffer at pH 5.70

4.1 $Ru(TMP)_2Cl_2$ Synthesis

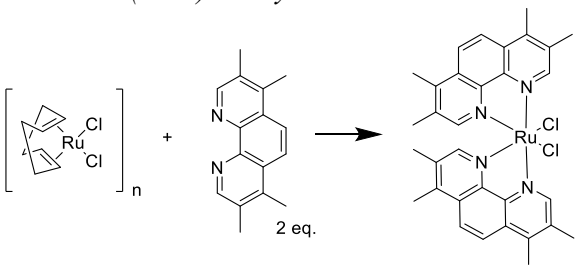

	Dichloro(1,5-cycooctadiene) Ru (II)	3,4,7,8 Tetramethyl-1,10 Phenanthroline	$Ru(TMP)_2Cl_2$,
Mass (mg)	206	341.5	71.5
Moles (mmol)	0.735	1.45	0.114
Molecular Mass (g/mol)	280.16	236.31	624.68

The precursor for $[Ru(TMP)_2(DPPZ\text{-}CN)]$, **$Ru(TMP)_2Cl_2$**, was first synthesized in the microwave at 140°C for 45 minutes. This was purified by washing with water because the tris(Me_4Phen) is water soluble, but the bis(Me_4Phen) is not very soluble in any solvent so could be dried with diethyl ether and collected. The product was run through the mass spectrometer to determine its identity and was assumed to be precursor, then it was taken into the follow-up reaction.

4.2 $Ru(TMP)_2(DPPZ\text{-}CN)$ Synthesis:

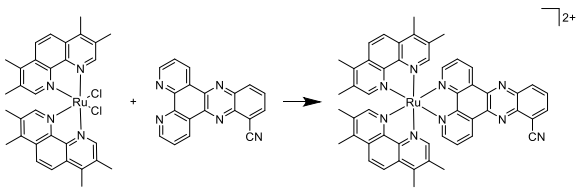

Since the complex was not made in the first synthesis, it was repeated using a different method. $Ru(TMP)_2Cl_2$ (160 mg, 0.256 mmol) and DPPZ-CN (86.6 mg, 0.282 mmol) were combined with 7 mL equal parts H_2O:Ethanol and microwaved for 45 minutes at 140°C. The solution was filtered with added PF_6 salt and 1561 mg was collected. A silica column using the same eluent as before was used and purification using Amberlite 402 was also performed with the fractions collected overnight in order to do an ion exchange from a $(PF_6)_2$ salt to a Cl_2 salt. The purified solutions were weighed; fractions 5 and 6 weighed 205 mg and fractions 1-4 weighed 175 mg, and then were run through the H-NMR using DMSO as the solvent. Fractions 1-4 were determined to contain the complex and the solution was divided into two flasks, $(PF_6)_2$ salt was added to one flask and produced 97 mg of product and the flask containing the Cl_2 salt was placed on the rotary evaporator and 47 mg of $[Ru(TMP)_2(DPPZ\text{-}CN)]$ were collected.

4.3 Sample preparation

Nucleic Acid	Abbreviations	Extinction Coefficient ($M^{-1}cm^{-1}$)
Deoxyribonucleic Acid	DNA	6600
Guanosine Monophosphate	GMP	11800
$(G_4T_4G_4)_2$	G_4T_4	383016
AGGGTT	Human Telomere G-Quadruplex	198450
C_5T_3		186570
C_{30}		222500

In general, solutions were prepared from a 10 mM phosphate buffer of varying KCl concentration and pH. The G-quadruplex solutions used 100 mM KCl in order to encourage the formation of the folded structure. In the case of the i-motif structures, they were in a monobasic buffer solution at pH= 5.70 to promote stability of the structures.

4.4 Preparation of DNA Stocks

DNA solutions were vortexed and sonicated to ensure a homogenous solution and the concentration of each DNA stock was determined by UV-Visible using the Beer-Lambert Law,

$$A = \varepsilon * c * 1,$$

where:

A = absorbance
ε = extinction coefficient (table 1 below)
C = concentration
1 = path length, a cuvette with path length of 1 was used for all titrations

	$Ru(TMP)_2Cl_2$	DPPZ-CN	$[Ru(TMP)_2(DPPZ\text{-}CN)]$
Mass (mg)	160	86.6	1561
Moles (mmol)	0.256	0.282	1.675
Molecular Mass (g/mol)	624.68	307.33	932.01

Table 1. Extinction Coefficients for Various Nucleic Acids Used:

5. APPENDIX

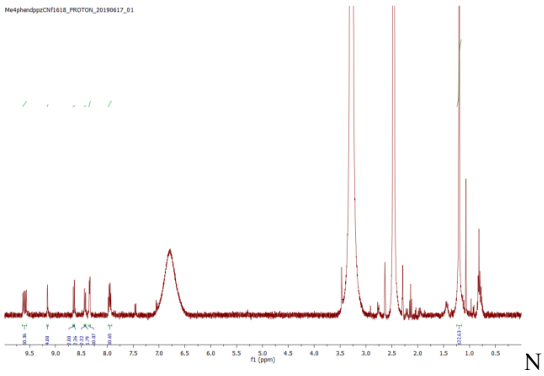

Figure 5.1 MR Spectroscopy Data for Synthesis through Refluxing

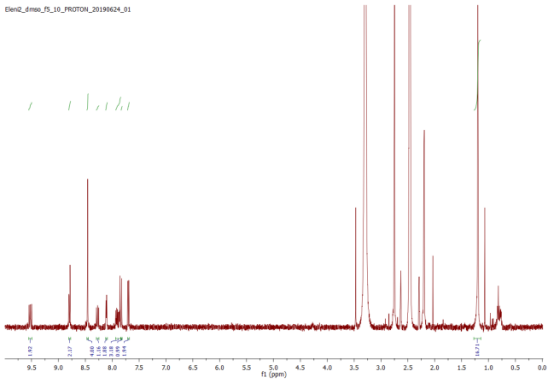

Figure 5.2 NMR Spectroscopy Data of Fractions 5 and 6

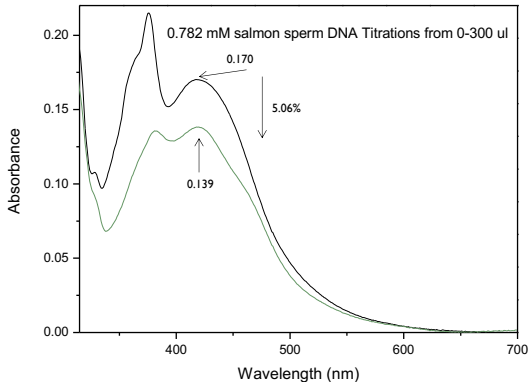

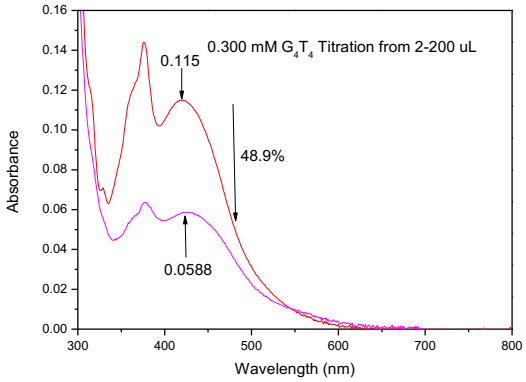

	0.782 mM ss DNA	1.98 mM ss DNA	3.88 mM GMP	0.300 mM G4T4	0.0311 mM HT G4	0.119 mM C5T3	
Highest Peaks Ratio	1.26:1	1.28:1	1.28:1	1.25:1	1.29:1	1.71:1	1.24:1
Lowest Peaks Ratio	0.986:1	0.945:1	1.24:1	1.08:1	1.28:1	1.08:1	1.20:1

Table 2. Ratios of the MLCT Bands Highest and Lowest Peaks

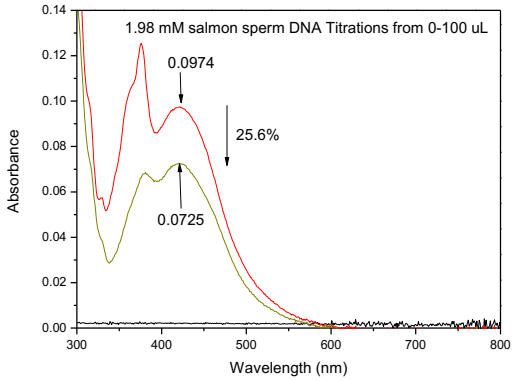

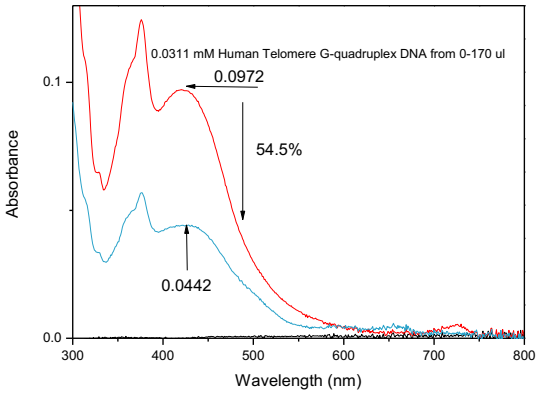

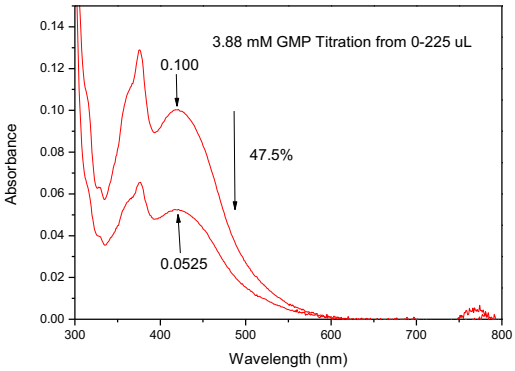

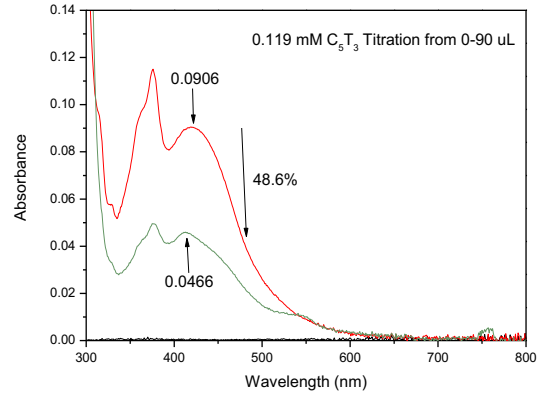
0.119 mM C5T3 Titration from 0-90 uL
0.0906
48.6%
0.0466
Absorbance
Wavelength (nm)

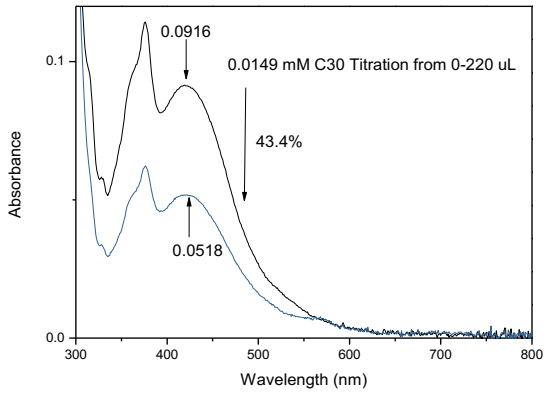
0.0916
0.0149 mM C30 Titration from 0-220 uL
43.4%
0.0518
Absorbance
Wavelength (nm)

7. REFERENCES

[1] Alberts, B.; Johnson, A.; Lewis, J, et al. The Structure and Function of DNA. *Molecular Biology of the Cell,* **2002**, 4.

[2] Aleksic, M. M.; Kapetanovic, V. An Overview of the Optical and Electrochemical Methods for Detection of DNA- Drug Interactions. *Acta Chim. Slov.,* **2014,** *61*, 555-573

[3] Assi, H. A.; Garavís, M.; González, C.; Damha, M. J. i-Motif DNA: Structural Features and Significance to Cell Biology. *Nucleic Acids Research,* **2018**, *46*(16), 8038–8056.

[4] Bhasikuttan, A. C.; Mohanty, J. Targeting G-quadruplex structures with extrinsic fluorogenic dyes: promising fluorescence sensors. *Chem. Commun.,* **2015,** *51,* 7581-7597.

[5] Bochman, M. L.; Paeschke, K.; Zakian, V. A. DNA Secondary Structures: Stability and Function of G-Quadruplex Structures. *Nature Reviews Genetics,* **2012**, *13*(11), 770–780.

[6] Boynton, A. N.; Marcélis, L.; Barton, J. K. [Ru(Me4phen)2dppz]2 , a Light Switch for DNA Mismatches. *Journal of the American Chemical Society,* **2016**, *138*(15), 5020–5023.

[7] Chen, T.; Mei, W.-J.; Wong, Y.-S.; Liu, J.; Liu, Y.; Xie, H.-S.; Zheng, W.-J. Chiral Ruthenium Polypyridyl Complexes as Mitochondria-Targeted Apoptosis Inducers. *MedChemComm,* **2010**, *1*(1), 73–75.

[8] Garcia-Ramos, J.C.; Galindo-Murillo, R.; Cortes-Guzman, F.; Ruiz-Azuara, L. Metal-Based Drug-DNA Interactions. *Journal of the Mexican Chemical Society,* **2013**, *57*(3).

[9] Georgiades, S. N.; Abd Karim, N. H.; Suntharalingam, K.; Vilar, R. Interaction of Metal Complexes with G-Quadruplex DNA. *Angewandte Chemie International Edition,* **2010**, *49* (24), 4020–4034.

[10] Hardison, R. C.; Chu, T. Ming. B-Form, A-Form, and Z-Form of DNA. *Working with Molecular Genetics,* **2019**, 2.5.

[11] Joshi, K.R.; Rokivadiya, A.J.; Pandya, J.H. Synthesis and Spectroscopic and Antimicrobial Studies of Schiff Base Metal Complexes Derived from 2-Hydroxyl-3-methoxy-5-nitrobenxaldehyde. *International Journal of Inorganic Chemistry,* **2014**, *2014*, 8.

[12] Li, G.; Sun, L.; Ji, L.; Chao, H. Ruthenium(II) complexes with dppz: from molecular photoswitch to biological applications. *Chem. Commun,* **2015**, *51*, 7581-7597.

[13] Li, H.-M. L.; Qiong Wu, X.-C. W.; Qi Wang, S.-Y. Z. A Ruthenium(II) complex as a potential luminescent switch-on probe for G-quadruplex DNA. *RSC Adv.,* **2017**, *7*, 23727-23734.

[14] Liu, J.; Zhang, C.; Rees, T. W.; Ke, L.; Ji, L.; Chao, H. Harnessing Ruthenium(II) as Photodynamic Agents: Encouraging Advances in Cancer Therapy. *Coordination Chemistry Reviews,* **2018**, *363*, 17–28.

[15] Mari, C.; Pierroz, V.; Ferrari, S.; Gasser, G. Combination of Ru(ii) complexes and light: new frontiers in cancer therapy. *Chem. Sci.,* **2015**, 6, 2660-2686.

[16] Metcalfe, C.; Thomas, J. A. Kinetically Inert Transition Metal Complexes That Reversibly Bind to DNA. *Chem. Inform,* **2003**, *32*(4), 215-224.

[17] Murnaghan, I. The Importance of DNA. *Explore DNA*, **2019**.

[18] NIH. The Francis Crick Papers: The Discovery of the Double Helix, 1951-1953. *U.S. National Library of Medicine,* **2015**.

[19] Pages, B. J.; Ang, D. L.; Wright, E. P.; Aldrich-Wright, J. R. Metal Complex Interactions with DNA. *Dalton Transactions,* **2015**, *44*(8), 3505–3526.

[20] Qu, X.; Trent, J. O.; Fokt, I.; Priebe, W.; Chaires, J. B. Allosteric, Chiral-Selective Drug Binding to DNA. *Proceedings of the National Academy of Sciences,* **2000**, *97*(22), 12032–12037.

[21] Rescifina, A.; Zagni, C.; Varrica, M. G.; Pistara, V.; Corsaro, A. Recent Advances in Small Organic Molecules as DNA Intercalating Agents: Synthesis, Activity, and Modeling. *European Journal of Medicinal Chemistry,* **2013**, *74*(19).

[22] Sinden, R. R. DNA Bending. *DNA Structure and Function,* **2012**, *282*, 58–94.

[23] Suntharalingam, K.; White, A. J. P.; Vilar, R. Two Metals Are Better than One: Investigations on the Interactions between Dinuclear Metal Complexes and Quadruplex DNA. *Inorganic Chemistry,* **2010**, *49*(18), 8371–8380.

[24] United States Department of Health and Human Services. DNA Base Pairing. *National Human Genome Research Institute,* **2017.**

[25] Hou, Jinqang et al. New insights from molecular dynamic simulation studies of the multiple binding modes of a ligand with G-quadruplex DNA. *Journal of Computer-Aided Molecular Design,* **2012**, *26*(12).

[26] Day, Henry Albert et al. i-Motif DNA: structure, stability and targeting with ligands. *Bioorganic & Medicinal Chemistry*, **2014**, *22*(16), 4407-18

[27] Cardin et al. *Chem. Sci.*, 2017,8, 4705-4723